Analysis and Characterization of a Wide-Angle Impedance Matching Metasurface for Dipole Phased Arrays

Trevor R. Cameron, *Member, IEEE,* and George V. Eleftheriades, *Fellow, IEEE*

***Abstract*—The effects of mutual coupling impact the performance of phased arrays as the beam is scanned off broadside. Wide-angle impedance matching (WAIM) alleviates this problem from a transmission-line impedance matching viewpoint, increasing the useable scan range of the array. Traditionally, a dielectric slab is placed at some distance above the array, resulting in a match at some given angle off broadside. We propose a simpler and more effective solution, replacing the dielectric slab with an ultra-thin metasurface composed of a sheet of split-ring resonators to improve the scanning characteristics of a dipole phased array. It is shown that the presence of the metasurface results in significant improvements in multiple scan planes. A generalised equivalent transmission-line model is introduced for the classical WAIM configuration and adapted for the metasurface. A quasi-analytical model based on the equivalent transmission-line model and the extracted scattering parameters of the metasurface properly predicts the scan range of the full structure, and allows for an accelerated design process.**

***Index Terms*—Antenna theory, phased arrays, dipole arrays, metasurfaces, metamaterials, periodic structures, impedance matching.**

I. Introduction

PHASED antenna arrays are highly desirable in applications such as radar, point-to-point, and satellite communication systems. The ability to scan the beam electronically is arguably the most attractive feature of phased arrays, as it is significantly more agile than its mechanical counterpart. Further, the integrated feeding mechanism negates the need for a secondary outer feed which would add bulk, weight, and possible blockage to the array.

However, it is well known that phased arrays suffer from degradation in transmitted power as the beam is scanned off broadside [1]. Wheeler's current sheet model [2] is often cited as a useful and insightful model for wideband arrays. The model is the limiting case of tightly packed dipoles backed by a ground plane. It predicts that the element resistance associated with the array will vary with $\cos\theta$ and $1/\cos\theta$ in the E- (electric, or transverse magnetic (TM)) and H- (magnetic, or transverse electric (TE)) planes, respectively. The transmitted power drops as the beam is scanned off broadside as a result of this variation in element resistance. At the limiting case of scanning to the horizon, the transmitted power drops to zero in all scan planes. Further, practical implementations of phased arrays exhibit a variation in both reactance and resistance as the beam is scanned [3], [4].

Early approaches to address this issue include loading the individual antenna elements with dielectric linings [5] or a number of dielectric disks [6]. These approaches require the alteration of all the elements in the array, which adds complexity and increased cost to the array. Further, this approach only works for certain types of array elements (e.g. waveguide antennas). Currently, the most common approach is the use of large radomes over the phased array [7]. These radomes are typically expensive to manufacture, and add significant bulk and weight to the array.

Viewing this limitation as an impedance matching problem, Magill and Wheeler proposed the method of wide-angle impedance matching (WAIM) [8]. The method introduces a thin, high permittivity dielectric sheet located at some distance above the array (Fig. 1). The sheet effectively acts as a shunt susceptance [9]. A sheet of the proper thickness and material properties, located at the right distance above the array, results in an impedance match at one or more scan angles. In [8], a waveguide array is loaded with a WAIM sheet, and it is shown that there is an improved match at three chosen scan angles, one in each of the E-, D- (diagonal or intercardinal), and H-planes. However, the impact of the WAIM sheet on the rest of the scan planes is neither shown nor discussed.

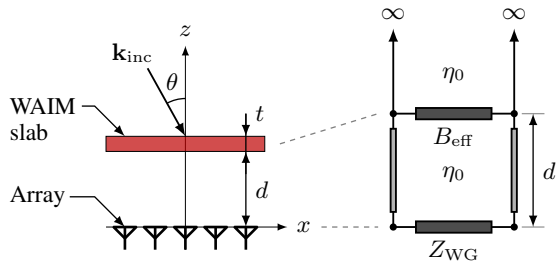

Fig. 1. Cross-sectional schematic (left) and equivalent transmission-line model (right) for a phased array compensated with a dielectric sheet. All impedances shown are functions of polarization (TE / TM), scan angle θ, and scan plane ϕ.

The concept of WAIM is fundamentally based on impedance matching, hence it follows naturally that a multilayer WAIM structure allows for increased bandwidth, being analagous to a multi-section impedance transformer [10]. In [11], a two-layer WAIM structure is designed for a tightly coupled

This research was supported by the Natural Sciences and Engineering Research Council of Canada (NSERC).

The authors are with the Edward S. Rogers Sr. Department of Electrical and Computer Engineering, University of Toronto, Toronto, ON M5S 3G4, Canada.

Digital Object Identifier XX.XXXX/TAP.2014.XXXXXXX

This article has been accepted for publication in a future issue of this journal, but has not been fully edited. Content may change prior to final publication. Citation information: DOI 10.1109/TAP.2015.2448231, IEEE Transactions on Antennas and Propagation

capacitively interconnected dipole array backed by a ground plane. The purpose in the investigation presented in [11] is a broadband (2–18 GHz), rather than wide-angle scanning, array. The design is optimized using custom periodic method of moments (PMM) code, as well as commercial solvers. Measurements are presented which align well with simulation results.

Recent work has proposed replacing the dielectric slab with a metamaterial slab [12]. The slab is both electrically and magnetically uniaxial, and designed for an array of circular waveguides. It is shown that, in theory, the use of the tangential and longitudinal permittivity and permeability components allowed for an improved match. However, the use of all components of the permittivity and permeability tensors results in a structure that is very difficult to physically realize. Simulation results for a simplified realisable structure making use of the tangential permittivity components are presented for the H-plane alone.

Most recently, the application of more sophisticated optimization techniques have been applied to multilayer metamaterial WAIM structures. In [13], the use of a multiple-agent stochastic global optimizer is proposed, specifically for a WAIM structure composed of a stack of periodically printed layers. In [14], the use of a particle swarm optimizer is proposed to optimize a multilayer WAIM structure, each layer being uniaxial, for an array of circular waveguides. Simulation results show significant improvement in scanning performance over a 1 GHz bandwidth centered at 15 GHz. However, a physical realization of the material parameters resulting from the optimization is not presented.

We propose to extend and generalise the work presented in [8] and [12]. A simpler and more effective solution is introduced, replacing the dielectric slab with an ultra-thin metasurface composed of subwavelength split-ring resonators (SRRs). Since the SRR response relies on a magnetic vector normal to the plane containing the rings [15], it is expected that this metasurface can be engineered to improve the scan range of the array in the H- and D-planes. The subwavelength nature of the rings makes them effectively invisible in the E-plane. It should be noted that the authors presented a proof of concept of this idea in [16]. The work presented here is a substantial extension to that paper, as will soon be apparent.

The phased array chosen for this study is an infinite array of dipoles. Dipole arrays are thin, low-profile, and lightweight. With the advent of printed technologies, dipole arrays are also remarkably cost-effective when compared to alternative array geometries. Further, circular polarization is relatively easy to achieve with crossed-dipole arrays. Finally, the advantage of a metasurface over the traditional dielectric slab becomes much more appreciable when working with dipole arrays. Reducing the bulk and weight associated with dielectric slabs keeps the compensated dipole array as thin and lightweight as possible.

The use of a dipole array also allows for an accurate analytical solution. In the analysis of waveguide arrays, the assumption is made that the presence of the WAIM sheet does not alter the input impedance of the waveguides themselves. The analysis presented in this paper is based on the driving (later called *scan*) impedance of the array, and by its very nature takes into account the impact of the WAIM sheet on the array elements. As a result, the analysis yields exact results, notwithstanding the assumptions made in the model.

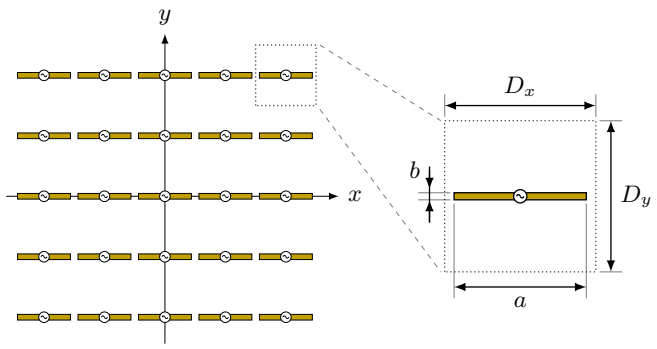

Fig. 2. Top-down view of the dipole array geometry (left) and unit cell with dimensions (right).The analysis presented in this paper assumes that the array is infinite in extent.

We begin by introducing an equivalent transmission-line model generalising classical WAIM techniques as applied to dipole arrays in Section II. The transmission-line model is then adapted for a metasurface. Both models are numerically validated using a full-wave solver in Section III, where excellent agreement is shown between the models and the full-wave solutions. The performance of the two structures are compared, and the physical behaviour of the metasurface is discussed in Section IV. Finally, the paper is summarized and concluded.

II. Analytical Model

A. Dipole Array Scan Impedance

To determine the reflection coefficient of the dipole array, it is first necessary to determine the scan impedance of the dipoles. The scan impedance is defined as the impedance seen looking into the terminals of a driven dipole element surrounded by an infinite array of similarly driven elements [17].

A top-down view of the array geometry and a unit cell with dimensions can be seen in Fig. 2. The dipole array is located in the xy-plane and the dipoles are x-oriented. It is assumed that the dipoles are thin, perfectly flat, and have a unidirectional (in x) cosinusoidal current distribution. All individual dipole elements are assumed to be excited with equal amplitudes and progressive phase shifts, allowing for the use of Floquet analysis. The dipole length and width are a and b, respectively. The array is assumed to be infinite in extent and located in free space. The array lattice is rectangular, and the spacing in x and y are D_x and D_y, respectively.

The analysis of the dipole array builds on that presented in [17], which in turn is based on that reported in [18]. The array is modeled as a current sheet, the complex power associated with a unit cell of the current sheet is evaluated, and the scan impedance is found to be

$$Z_S = \frac{2\eta}{\pi^2}\frac{\hat{a}^2}{\hat{D}_x\hat{D}_y}\sum_{m=-\infty}^{\infty}\sum_{n=-\infty}^{\infty} F_n^2\, G_m^2 H_{mn} \qquad (1)$$

This article has been accepted for publication in a future issue of this journal, but has not been fully edited. Content may change prior to final publication. Citation information: DOI 10.1109/TAP.2015.2448231, IEEE Transactions on Antennas and Propagation

where

$$F_n = \frac{\sin(\pi \hat{k}_{yn} \hat{b})}{\pi \hat{k}_{yn} \hat{b}} \tag{2a}$$

$$G_m = \frac{\cos(\pi \hat{k}_{xm} \hat{a})}{1 - (2\hat{k}_{xm} \hat{a})^2} \tag{2b}$$

$$H_{mn} = \frac{1 - \hat{k}_{xm}^2}{\hat{\kappa}_{mn}}\,. \tag{2c}$$

A short derivation of (1) and (2) is presented in the Appendix. Note that all dimensions are normalized with respect to the wavelength λ, and that all components of the wavenumbers are normalized with respect to the wavenumber k, hence the hat notation. In the case of the array being located in free space, which is the case for analysis presented here, these are the free-space wavelength and wavenumber λ_0 and k_0, respectively. The normalized Floquet wavenumbers are given by

$$\hat{k}_{xm} = \hat{k}_{x0} + \frac{m}{\hat{D}_x} \tag{3a}$$

$$\hat{k}_{yn} = \hat{k}_{y0} + \frac{n}{\hat{D}_y} \tag{3b}$$

$$\hat{\kappa}_{mn} = \begin{cases} \sqrt{1 - \hat{k}_{xm}^2 - \hat{k}_{yn}^2} & \text{if } \hat{k}_{xm}^2 + \hat{k}_{yn}^2 \leq 1 \\ -j\sqrt{\hat{k}_{xm}^2 + \hat{k}_{yn}^2 - 1} & \text{if } \hat{k}_{xm}^2 + \hat{k}_{yn}^2 > 1 \end{cases} \tag{3c}$$

where $\hat{k}_{x0} = \sin\theta\cos\phi$ and $\hat{k}_{y0} = \sin\theta\sin\phi$. The addition of a ground plane located at a distance h below the array can be taken into account by appending $(1 - \exp(-j4\pi\hat{\kappa}_{mn}h))$ to (1). This can be interpreted as an additional contribution from reflections off the ground plane, or from an image of the array across the ground plane.

The addition of a WAIM slab or metasurface above the array modifies (1), which now takes the form

$$Z_S = \frac{2\eta}{\pi^2} \frac{\hat{a}^2}{\hat{D}_x \hat{D}_y} \sum_{m=-\infty}^{\infty} \sum_{n=-\infty}^{\infty} F_n^2\, G_m^2 \times \left(H_{mn}^{\mathrm{TE}}\, \hat{\eta}_{mn}^{\mathrm{TE}} \gamma_{mn}^{\mathrm{TE}} + H_{mn}^{\mathrm{TM}}\, \hat{\eta}_{mn}^{\mathrm{TM}} \gamma_{mn}^{\mathrm{TM}} \right) \tag{4}$$

where

$$H_{mn}^{\mathrm{TE}} = \frac{\hat{k}_{yn}^2}{\hat{k}_{xm}^2 + \hat{k}_{yn}^2} \tag{5a}$$

$$H_{mn}^{\mathrm{TM}} = \frac{\hat{k}_{xm}^2}{\hat{k}_{xm}^2 + \hat{k}_{yn}^2} \tag{5b}$$

and the normalized Floquet impedances $\hat{\eta}_{mn}^{\mathrm{TE}}$ and $\hat{\eta}_{mn}^{\mathrm{TM}}$ are given by $1/\hat{\kappa}_{mn}$ and $\hat{\kappa}_{mn}$, respectively. The $\gamma_{mn}^{\mathrm{TE}}$ and $\gamma_{mn}^{\mathrm{TM}}$ terms in (4) cover additional contributions to the scan impedance due to reflections from nearby interfaces. For a general interface, these terms are not equivalent, as they are functions of $\hat{\eta}_{mn}^{\mathrm{TE}}$ and $\hat{\eta}_{mn}^{\mathrm{TM}}$, respectively, which themselves are functions of polarization, m, and n. Referring to (3), it is noted that in general, higher-order Floquet modes contain both TE and TM components regardless of the scan plane being considered, hence the need to recast (1) in the form seen in (4).

Due to the geometry of the dipole array (Fig. 2), the E- and H-planes in this context are aligned with the x- and y-axes, respectively, and the TE and TM polarizations are in y and x, respectively. Finally, it can readily be verified that in the case of a ground plane located at a distance h below the dipole array, (4) reduces to (1) appended with $(1-\exp(-j4\pi\hat{\kappa}_{mn}h))$, as presented in [17].

The scan impedance for a phased array of resonant dipoles with a ground plane located at $h = 1/4\,\lambda$ below the dipoles can be seen in Fig. 3. The mutual coupling is weakest in the E-plane where there is a small reactive component in the scan impedance across the scan range. Conversely, the mutual coupling is strongest in the H-plane, where the reactive component of the scan impedance is seen to increase dramatically with the scan angle θ.

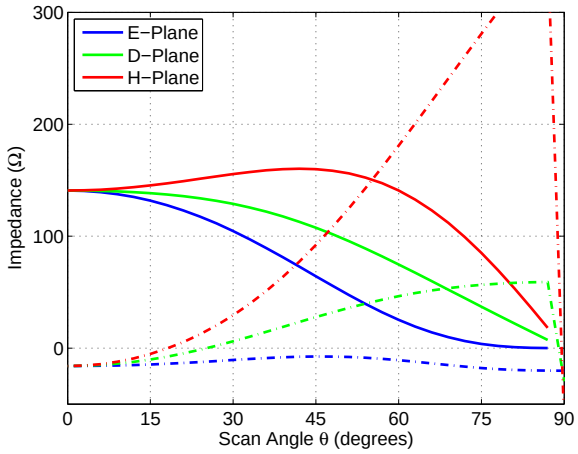

Fig. 3. Scan resistance (solid) and reactance (dashed) for an uncompensated dipole array backed by a ground plane.

The dipole is terminated to achieve maximum transmitted power at broadside. As a result, the reflection seen looking into the terminals of the dipoles is given by

$$\Gamma(\theta, \phi) = \frac{Z_b - Z_S(\theta, \phi)}{Z_b + Z_S(\theta, \phi)} \tag{6}$$

where $Z_b = Z_S(\theta = 0, \phi = 0)$ is the broadside scan impedance in the E-plane. This definition of the reflection coefficient is consistent with that seen in [19].

Note that the analysis presented in [2] and [8] determines the reflection as that seen by a plane wave looking in to the array (i.e the array is in receive mode). Conversely, the analysis presented here is done with respect to driving the array (i.e. transmit mode). The theorem of reciprocity ensures that both viewpoints are equivalent in the context of impedance matching [20].

B. Dielectric WAIM Slab Equivalent Transmission-Line Model

To take into account the presence of the dielectric WAIM slab (henceforth referred to as the dielectric slab) above a dipole array backed by a ground plane, a simple unit cell equivalent transmission-line model is introduced. As can be seen in Fig. 4, the dipole is located at a distance h above the

This article has been accepted for publication in a future issue of this journal, but has not been fully edited. Content may change prior to final publication. Citation information: DOI 10.1109/TAP.2015.2448231, IEEE Transactions on Antennas and Propagation

ground plane and a dielectric slab of thickness t is located at a distance d above the dipole. The section of transmission line representing the dielectric slab has an intrinsic impedance of η_1 which reflects the permittivity $\varepsilon = \varepsilon_r\,\varepsilon_0$ of the dielectric. It is assumed, without loss of generality, that the areas between the ground plane, dipole, and WAIM slab are free space. However, it is simple to replace the wave impedance for the relevant sections of transmission line with that of e.g., a dielectric spacer, in which case this analysis still holds.

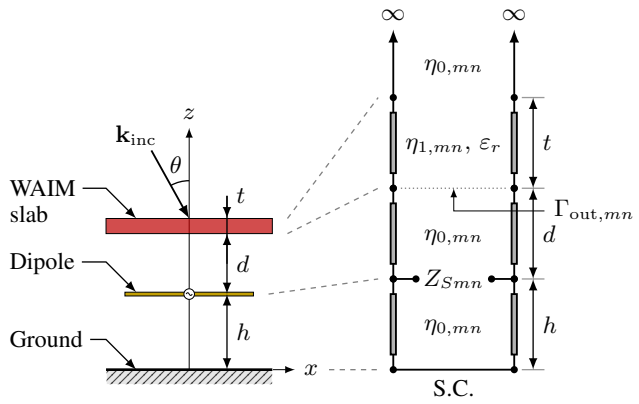

Fig. 4. Cross-sectional schematic (left) and equivalent transmission-line model (right) for a unit cell of a dipole array backed by a ground plane and loaded with a dielectric WAIM slab. To determine Z_S, it is necessary to sum over a number of Floquet impedances Z_{Smn}, as per (4) and Fig. 5. All impedances shown are functions of polarization (TE / TM), scan angle θ, and scan plane ϕ.

The unit cell seen in Fig. 4 applies for any individual (m, n) Floquet mode, yielding the corresponding Floquet impedance Z_{Smn}. The form of (4) suggests that the scan impedance Z_S consists of number of impedances connected in series, as illustrated in Fig. 5. In the case of the dielectric slab, the two-port WAIM networks seen in Fig. 5 represent the section of transmission line with impedance $\eta_{1,mn}$ in Fig. 4.

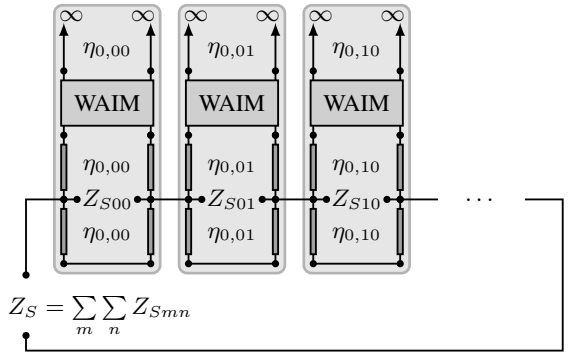

Fig. 5. Equivalent transmission-line model illustrating the series summation of individual Floquet impedances to determine the scan impedance of a dipole array backed by a ground plane and loaded with a WAIM structure. To determine Z_S, it is necessary to sum over a number of Floquet impedances Z_{Smn}, as per (4). All impedances shown are functions of polarization (TE / TM), scan angle θ, and scan plane ϕ.

As a result of the interfaces above and below the dipole, a series of multiple reflections occur. Some algebraic manipulation results in a pair of geometric series, which can then be simplified to

$$\gamma_{mn}^{\text{TE/TM}} = \left(1 + \Gamma_{\text{out},mn}^{\text{TE/TM}} \exp\left(-j4\pi\hat{\kappa}_{mn} d\right)\right) \times \frac{1 + \Gamma_g \exp\left(-j4\pi\hat{\kappa}_{mn} h\right)}{1 - \Gamma_{\text{out},mn}^{\text{TE/TM}} \Gamma_g \exp\left(-j4\pi\hat{\kappa}_{mn}(d+h)\right)} \quad (7)$$

where $\Gamma_g = -1$ is the reflection coefficient associated with the ground plane. The reflection seen looking into the dielectric slab is given by

$$\Gamma_{\text{out},mn}^{\text{TE/TM}} = \frac{\Gamma_{01,mn}^{\text{TE/TM}} + \Gamma_{10,mn}^{\text{TE/TM}} \exp\left(-j4\pi\hat{\kappa}_{mn} t\right)}{1 + \Gamma_{01,mn}^{\text{TE/TM}} \Gamma_{10,mn}^{\text{TE/TM}} \exp\left(-j4\pi\hat{\kappa}_{mn} t\right)} \quad (8)$$

where $\Gamma_{01,mn}^{\text{TE/TM}}$ and $\Gamma_{10,mn}^{\text{TE/TM}}$ are the Fresnel reflection coefficients associated with the η_0 and η_1 interfaces.

This model relaxes the restriction stated in [8], namely that the sheet be thin and have a high permittivity. Further, the model is easily adapted for multiple WAIM layers by adding sections of transmission line associated with the additional WAIM layers (and possibly air gaps) to the transmission-line model in Fig. 4. The only change in the analytical expressions would involve additional impedance/reflection coefficient transformations to properly evaluate $\Gamma_{\text{out},mn}^{\text{TE/TM}}$, seen in (8).

C. WAIM Metasurface Equivalent Transmission-Line Model

The dielectric slab is now replaced with a sheet of subwavelength SRRs. A top-down view of a unit cell of the dipole array loaded with the WAIM metasurface (henceforth referred to as the metasurface), as well as the dimensions of a unit cell of the metasurface itself, can be seen in Fig. 6.

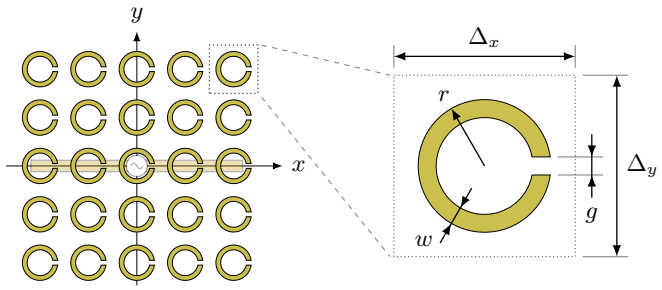

Fig. 6. Top-down view of a unit cell of the dipole array loaded with the metasurface (left) and a unit cell of the metasurface with dimensions (right).

The transmission-line model seen in Fig. 4 is amended to take into account the metasurface by replacing the section of transmission line representing the dielectric slab with a shunt impedance Z_W representing the metasurface. The amended unit cell equivalent transmission-line model can be seen in Fig. 7. In previous metamaterial circuit models, the magnetic component of the metamaterial is modeled by a series element [21]. This is seen again in recent work specific to metasurfaces [22]. In both contexts, the rings (or SRRs) are oriented perpendicular to the metasurface and are excited by a magnetic vector that is tangential to the surface. Here, the SRRs lie parallel to the surface and are excited by a magnetic vector that is normal to the surface, hence the shunt representation in Fig. 7.

This article has been accepted for publication in a future issue of this journal, but has not been fully edited. Content may change prior to final publication. Citation information: DOI 10.1109/TAP.2015.2448231, IEEE Transactions on Antennas and Propagation

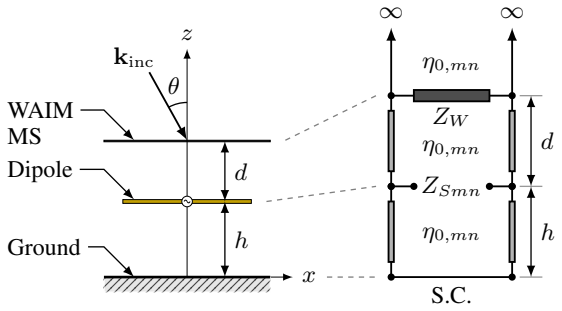

Fig. 7. Cross-sectional schematic (left) and equivalent transmission-line model (right) for a unit cell of a dipole array backed by a ground plane and loaded with a WAIM metasurface. To determine Z_S, it is necessary to sum over a number of Floquet impedances Z_{Smn}, as per (4) and Fig. 5. All impedances shown are functions of polarization (TE / TM), scan angle θ, and scan plane ϕ.

As in the case of the dielectric slab, the unit cell seen in Fig. 7 applies for any individual (m, n) Floquet mode. In this case, the two-port WAIM networks seen in Fig. 5 represents the metasurface shunt impedance seen in Fig. 7.

The $\gamma_{mn}^{\text{TE/TM}}$ terms seen in (7) are still valid. However, $\Gamma_{\text{out},mn}^{\text{TE/TM}}$ is now the reflection seen looking into a shunt connection of the corresponding metasurface impedance $Z_W^{\text{TE/TM}}$ and the free-space wave impedance located above the sheet. At this point, it is necessary to employ a full-wave solver to extract the equivalent impedance associated with the metasurface, as there is no readily available analytical model for the impedance associated with a sheet of rings. A waveguide simulation of the metasurface alone yields the S-parameters, from which the equivalent impedance can be computed.

The periodicity (and, as it follows, the lattice spacing) of the metasurface is significantly smaller than that of the dipole array. As a result, the metasurface is treated as a homogenized structure. The use of a single metasurface impedance Z_W for all Floquet modes in the transmission-line model is intuitively analogous to the use of a single relative permittivity ε_r in the case of a dielectric WAIM slab. Previous investigations characterizing periodic frequency selective surfaces (FFSs), which are similar to metasurfaces, use a multi-mode equivalent network [23]. The FSS is treated on a (Floquet) mode by mode basis. Here, however, there are two periodic structures (the dipole array and the metasurface) with significantly different periodicities, hence the use a homogenized impedance for the structure with the smaller periodicity.

Whether the array is being driven or illuminated, a number of higher-order Floquet modes will be excited on the metasurface. It is thus necessary to include a number of higher-order modes in the metasurface impedance extraction simulation to achieve accurate results.

Negligible coupling has been observed between the Floquet modes, and as a result, they can be characterized by their individual two-port S-parameter matrices. The S-parameters are extracted from the full-wave simulation, properly de-embedded, and mapped to their equivalent impedance matrices [10]. Noting that (1) can be interpreted as a series combination of the Floquet impedances, a similar approach is taken with the Floquet impedances computed from the extracted simulation S-parameters. Each Floquet mode is represented by a T-network associated with its impedance matrix, and they are added in series. This process is done individually for TE and TM polarizations, yielding Z_W^{TE} and Z_W^{TM}, respectively. This process is illustrated schematically in Fig. 8.

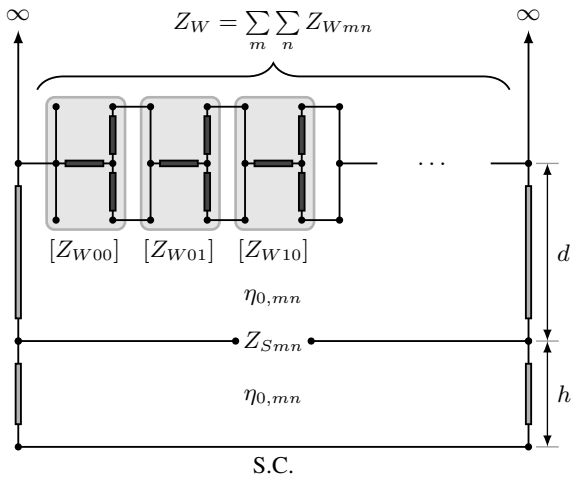

Fig. 8. Detailed equivalent transmission-line model for a unit cell of a dipole array backed by a ground plane and loaded with a WAIM metasurface. To determine Z_S, it is necessary to sum over a number of Floquet impedances Z_{Smn}, as per (4) and Fig. 5. The T-networks associated with the (m,n) Floquet modes are mapped from the S-parameters extracted from full-wave simulations. All impedances shown are functions of polarization (TE / TM), scan angle θ, and scan plane ϕ.

III. Numerical Validation

The equivalent transmission-line models allow for the analysis of the dipole array loaded with the dielectric slab and the metasurface. However, in both cases, all degrees of freedom are within an infinite sum. A brute force approach has been employed, scanning the degrees of freedom, such as geometry and material parameters, over ranges of achievable values. To determine the best case geometry, the relative transmitted power (or transmittance), computed as $T = 1 - |\Gamma|^2$, is monitored in all scan planes. The transmittance is averaged across the scan range in the H- and D-planes, while ensuring that the transmittance within that range does not drop below 0.8, and that the impact on the E-plane is negligible. The geometry with the largest scan range fitting the listed criteria is then chosen. It has been found that to achieve accurate results, the Floquet modes spanning $m, n \in \{-10, -9, \ldots, 9, 10\}$ are required (at least) for both TE and TM polarizations when using the transmission-line models. The number of modes required when using the transmission-line model has been found to be dictated mostly by the presence of the dipole itself, rather than nearby interfaces such as the dielectric slab or metasurface.

The metasurface model does require that full-wave simulations be run before one can use the transmission-line model, as outlined in Section II-C. With that said, simulations involving the metasurface alone are significantly less computationally intensive than the entire structure, comprising the dipole,

This article has been accepted for publication in a future issue of this journal, but has not been fully edited. Content may change prior to final publication. Citation information: DOI 10.1109/TAP.2015.2448231, IEEE Transactions on Antennas and Propagation

ground plane, and metasurface. The metasurface is simulated using ANSYS High Frequency Structural Simulator (HFSS), a commercial finite element method solver. Periodic boundary pairs are used to model an infinite metasurface and allow for scanning the incident angle and scan plane. A pair of Floquet ports are used to determine the S-parameters as a function of scan angle and scan plane. The SRRs are modeled using perfect electrical conductors (PECs).

It has been found that for this metasurface, ten modes are necessary to accurately model the metasurface impedance. In addition to the two specular (or propagating) modes TE_{00} and TM_{00}, the $(m,n) = (\pm 1, 0)$ and $(0, \pm 1)$ modes for both TE and TM polarizations are included in the simulation. Note that fewer modes are necessary to achieve accurate results for the HFSS metasurface simulation when compared to the transmission-line model. This is assumed to be due to the more complex interaction between the dipoles and the metasurface due to the sub-wavelength spacing between them.

Using the best case results yielded by the parameter scan, the entire structure is simulated using HFSS. Master/slave boundary pairs are used to model the infinite array and vary the scan angle and scan plane. The ground plane and dipole are modeled with PECs. The dimensions as per Fig. 2 are an array spacing $D_x = D_y = 1/2\,\lambda$, and dipole dimensions of $a = 48/100\,\lambda$ by $b = 1/50\,\lambda$. The dipole is driven by a lumped port and the top of the simulation space is terminated with a perfectly matched layer (PML). The ground plane is located $h = 1/4\,\lambda$ below the dipole, and the entire structure is modeled in free space. The design frequency for the full-wave simulations has been chosen to be 10 GHz.

The chosen metric to evaluate the performance of the various designs presented in the following sections is the relative transmitted power. Note that the broadside impedance, used to compute the reflection coefficent as per (6), varied over a small range as the WAIM geometry is altered. Should one desire to apply a formal optimization process to the design, the broadside impedance could be set to, e.g., the uncompensated dipole broadside impedance ($Z_b^{\mathrm{UC}} = 140.8 - j9.3\,\Omega$) without severely compromising the optimization process.

A. Dielectric WAIM Slab

Analytical and simulation results for the best case dielectric slab can be seen in Fig. 9. The dielectric slab is modeled as a lossless dielectric with a relative permittivity $\varepsilon_r = 2.9$. The distance above the array and slab thickness are $d = 3/5\,\lambda$ and $t = 3/10\,\lambda$, respectively. Improvements in the H- and D-planes are observed, while there is almost no impact on the E-plane. Excellent agreement is seen between the analytical model and simulation results. The broadside impedance of the full structure is $Z_b^{\mathrm{DS}} = 130.7 - j11.6\,\Omega$.

It has been found that when using a dielectric slab, in general, increased scan ranges can be achieved in the H- and D-planes with minimal impact on E-plane performance. Conversely, solutions that offer increased scan range in the E-plane greatly reduce the useful scan range in the H- and D-planes. It has also been found that the improvement in any scan plane comes at the cost of an accelerated drop in transmitted power in scan ranges higher than the compensated scan region.

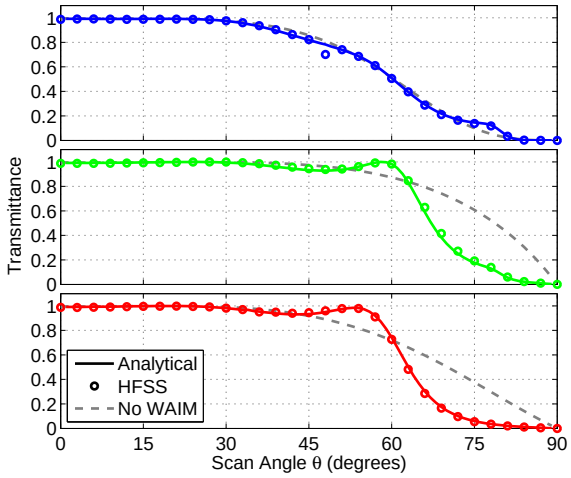

Fig. 9. Relative transmitted power as a function of scan angle in the E- (top), D- (middle), and H-planes for an infinite array of dipoles loaded with a dielectric WAIM sheet.

B. WAIM Metasurface

Analytical and simulation results for the best case metasurface can be seen in Fig. 10. The metasurface is modeled using SRRs composed of PEC sheets. The SRR lattice spacing is $\Delta_x = 1/10\,\lambda$ by $\Delta_y = 1/10\,\lambda$. The radius, width, and gap of the SRR are $r = 107/3000\,\lambda$, $w = 3/1000\,\lambda$, and $g = 29/2500\,\lambda$, respectively. The metasurface is located $d = 8/35\,\lambda$ above the dipole. An improved scan range is seen in the H- and D-planes, again with minimal impact on the E-plane. As in the case of the dielectric slab, excellent agreement is observed between the analytical model and simulation results. The broadside impedance of the full structure is $Z_b^{\mathrm{MS}} = 133.7 + j9.3\,\Omega$.

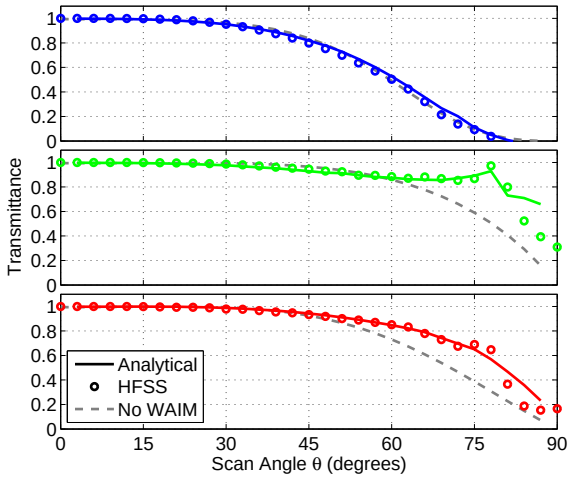

Fig. 10. Relative transmitted power as a function of scan angle in the E- (top), D- (middle), and H-planes for an infinite array of dipoles loaded with a WAIM metasurface.

A significant improvement is seen in the D-plane in particular, where approximately 90% relative transmitted power is observed at $\theta = 78°$. Further, the metasurface does not suffer from the accelerated drop in transmitted power beyond the

This article has been accepted for publication in a future issue of this journal, but has not been fully edited. Content may change prior to final publication. Citation information: DOI 10.1109/TAP.2015.2448231, IEEE Transactions on Antennas and Propagation

compensated scan range seen in the case of the dielectric slab. There is some disagreement between the full structure simulation and the transmission-line model at very high scan angles. The simulations from which the metasurface impedance used in the transmission-line model are extracted have issues with convergence at these angles, possibly due to the inclusion of several higher-order Floquet modes.

IV. Discussion

A. WAIM Performance

The ranges in which relative transmitted power is greater or equal to 80% for the uncompensated dipole array, the dielectric slab, and the metasurface are summarized in Table I. The metasurface allows for a larger scan range in the D- and H-planes when compared to its dielectric slab counterpart, while only losing 1° in the E-plane. In particular, the scan range in the D-plane is significantly improved.

TABLE I
WAIM Scan Ranges

	No WAIM	Dielectric Slab	Metasurface
E-plane	0 – 48°	0 – 46°	0 – 45°
D-plane	0 – 62°	0 – 63°	0 – 81°
H-plane	0 – 52°	0 – 59°	0 – 65°

Although the greatest improvement shown in Fig. 10 appears to occur in only one of the scan planes, there are two intercardinal planes when considering the entire azimuthal scan range. The additional scan range offered by the metasurface is better appreciated when overlaying plots of the regions in which 80% or more power is transmitted for the uncompensated array, the dielectric slab, and the metasurface. Referring to Fig. 11, it is clear that the metasurface has a more significant impact on the usable range of the dipole array when compared to the dielectric slab.

B. Metasurface Equivalent Impedance

To help elucidate the physical behaviour of the metasurface, as well as its interaction with the dipole array, the extracted TM and TE metasurface impedances are presented in Figs. 12 and 13, respectively. As is expected, the impedance is almost purely reactive across all scan planes for both polarizations. At extreme scan angles ($\theta > 80°$), a resistive component appears for both polarizations. This is assumed to be a numerical artifact. It has been confirmed that the resistive portion of the extracted impedances have a negligible impact on the analytical results; the inclusion of these resistive components when computing the scan impedance using (4) has no appreciable impact on the results.

Although there is a significant reactive component for both polarizations in all scan planes, it can be seen in Fig. 10 that the presence of the metasurface has a negligible impact on the E-plane. The impedance seen by the dipole array is not the metasurface impedance itself, but the metasurface impedance shunted with the free-space impedance behind the metasurface.

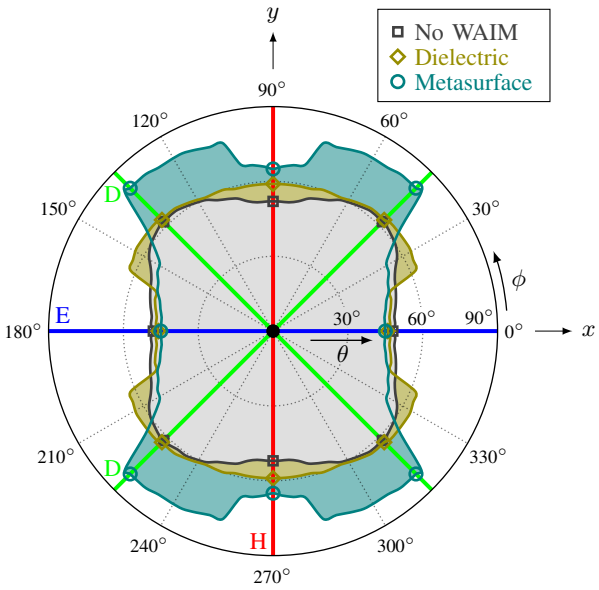

Fig. 11. Scan regions in which 80% relative transmitted power is achieved for an uncompensated array (gray, squares), the dielectric WAIM slab (olive, diamonds), and the WAIM metasurface (teal, circles). Also shown are the E-plane (blue), D-planes (green), and H-plane (red). The coordinate system reflects the geometry of the dipole array as seen in Fig. 2.

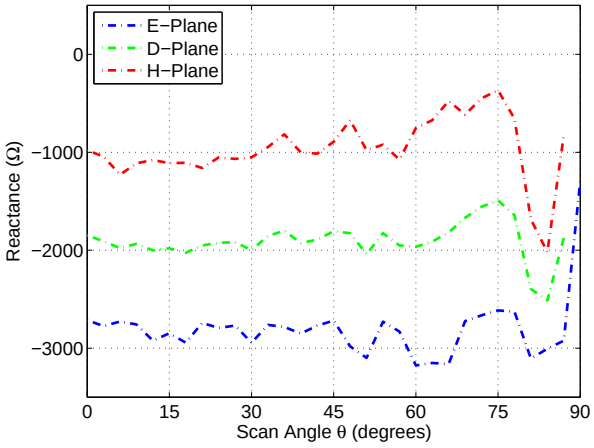

Fig. 12. Metasurface TM reactance as a function of scan angle.

These impedances, for TM and TE polarizations, can be seen in Figs. 14 and 15, respectively.

Referring to Fig. 14, it can be seen that for TM polarization, there is a very small reactive component associated with the metasurface impedance. Overall, the impedance seen looking into the metasurface with free space behind it appears almost entirely like a regular free-space TM wave impedance profile. This polarization dominates the E-plane response, and hence explains the minimal impact seen in that plane.

Conversely, referring to Fig. 15 where the metasurface is shunted with the free-space wave impedance, a very different behaviour is apparent. Although there is once again a very small reactive component near broadside, the impedance seen into the metasurface with free space behind it becomes increasingly reactive with increasing scan angle. As in the case

This article has been accepted for publication in a future issue of this journal, but has not been fully edited. Content may change prior to final publication. Citation information: DOI 10.1109/TAP.2015.2448231, IEEE Transactions on Antennas and Propagation

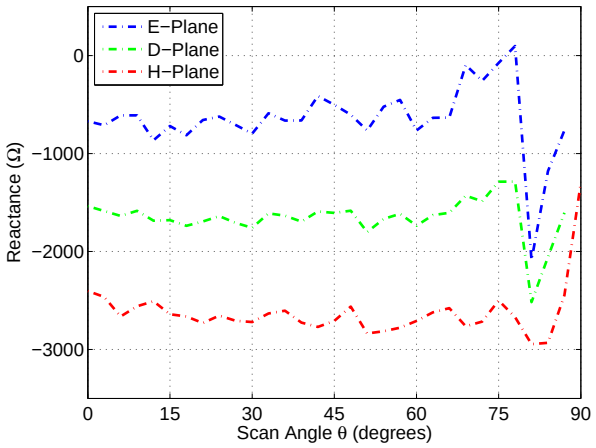

Fig. 13. Metasurface TE reactance as a function of scan angle.

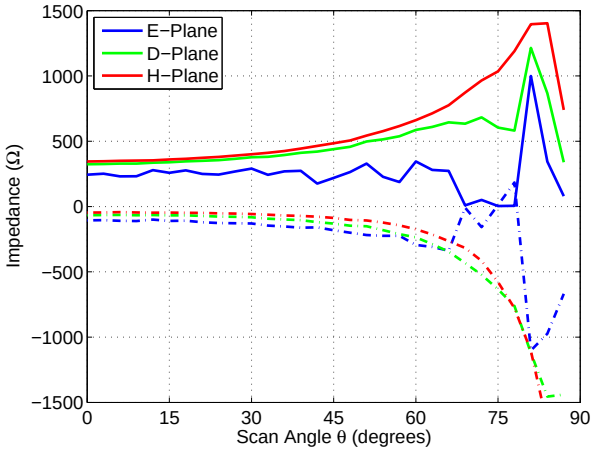

Fig. 15. Metasurface TE resistance (solid) and reactance (dashed), shunted with free-space wave impedance, as a function of scan angle.

of the TM polarization, the resistive component seen in Fig. 15 is very near that of a regular free-space TE wave impedance profile.

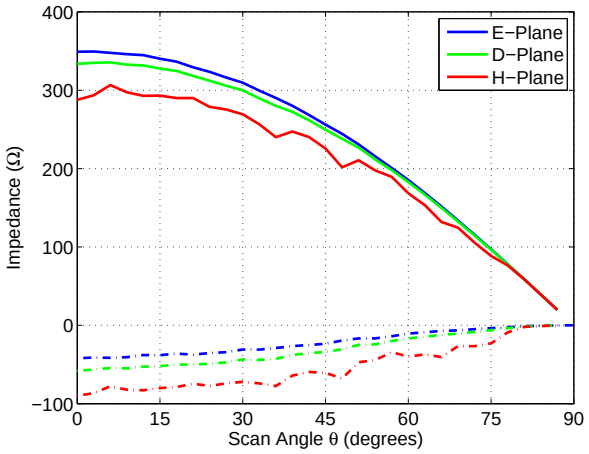

Fig. 14. Metasurface TM resistance (solid) and reactance (dashed), shunted with free-space wave impedance, as a function of scan angle.

Referring to the scan impedance of an uncompensated dipole array backed by a ground plane (Fig. 3), the reactance in the H-plane becomes increasingly inductive as the scan angle increases. This is the exact opposite profile as that seen in the TE reactance in Fig. 15. As this polarization dominates the H-plane response, it is now understandable from where the metasurface compensation arises.

The authors would like to stress that the view expressed in this subsection of the paper is a high level, intuitive view of the physical behaviour of the metasurface. It neglects details such as the interactions of the higher-order Floquet modes with the metasurface. It cannot be assumed that traditional impedance matching be applied using the uncompensated dipole array scan impedance with the extracted metasurface impedance. However, the discussion in this subsection does offer some physical insight as to the workings of the metasurface, and how it interacts with the dipole array.

C. Bandwidth

Simulations have been run at the design frequency (10 GHz) and 10% off the design frequency (9 and 11 GHz) to investigate the bandwidth of the uncompensated dipole array as well as the two WAIM structures. Results for the dielectric WAIM slab can be seen in Fig. 16. The dielectric slab performs well at lower scan angles, but suffers in middle scan angles. Overall, an observable fluctuation in transmitted power is seen across the scan range in all scan planes. The largest impact is seen in the E-plane at the lower frequency.

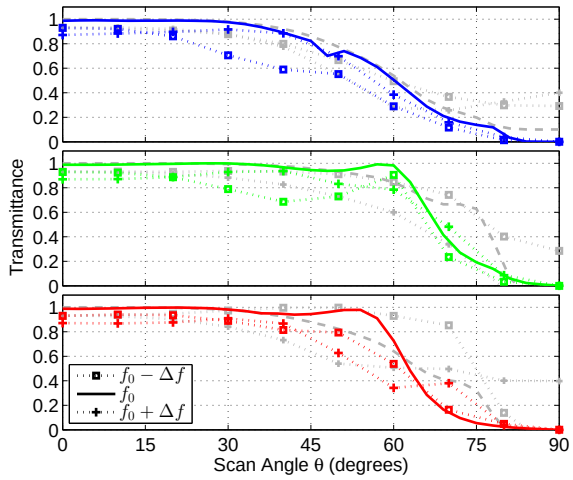

Fig. 16. Relative transmitted power as a function of scan angle in the E- (top), D- (middle), and H-planes for an infinite array of dipoles loaded with a dielectric WAIM sheet. Also shown in gray is the relative transmitted power for an uncompensated dipole array. The design frequency is f_0=10 GHz and Δf=1 GHz.

Results for the metasurface can be seen in Fig 17. Once again, the largest impact is seen in the E-plane at the lower frequency range. However, the metasurface is more consistent in all other scan planes and frequencies than the dielectric slab. Further, the metasurface performs remarkably well at high scan angles regardless of the frequency in all scan planes,

This article has been accepted for publication in a future issue of this journal, but has not been fully edited. Content may change prior to final publication. Citation information: DOI 10.1109/TAP.2015.2448231, IEEE Transactions on Antennas and Propagation

with the exception of the lower frequency in the E-plane. Approximately 70% relative transmitted power is observed in the D- and H-planes up to a scan angle of 80° at all three frequencies. These results indicate that in the case of a multilayer structure such as that seen in [11], [13], [14], fewer metasurface layers would be required when compared to the dielectric slab to achieve wider-band performance.

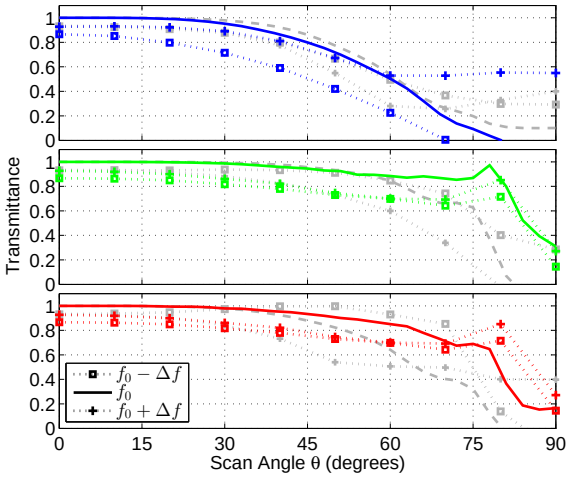

Fig. 17. Relative transmitted power as a function of scan angle in the E- (top), D- (middle), and H-planes for an infinite array of dipoles loaded with a WAIM metasurface. Also shown in gray is the relative transmitted power for an uncompensated dipole array. The design frequency is f_0=10 GHz and Δf=1 GHz.

V. Conclusion

A generalised transmission-line model for a unit cell of an infinite phased array of dipoles backed by a ground plane and loaded with a WAIM sheet has been presented. The model allows for the accurate analysis of the array loaded with a WAIM sheet consisting of a dielectric slab or an ultra-thin metasurface. Using this model, a dielectric WAIM slab and a WAIM metasurface have been designed and numerically validated with full-wave simulations. It has been shown that the metasurface offers significantly improved performance, while being very simple to implement. A structure making use of a simple sheet of SRRs increases the scan range in the D- and H-planes by 16° and 10°, respectively while having a negligible impact on the E-plane. Finally, the metasurface has been shown to have a better and more consistent bandwidth response than the dielectric slab. Over and above increased performance, the metasurface is better suited for dipole arrays due to its being very thin and lightweight, mirroring two of the most attractive traits associated with dipole arrays themselves.

Appendix
Derivation of the Scan Impedance

The derivation below is based on that found in [17] (pp. 247–252), which in turn is based on that presented in [24]. The array geometry, however, is now assumed to be a general skew-grid, as shown in Fig. 18. The dipoles are aligned along

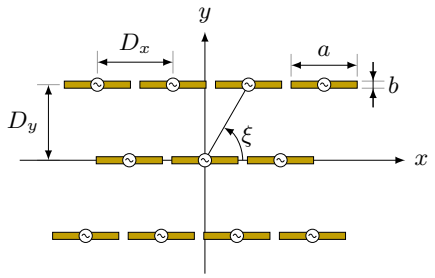

Fig. 18. Top-down view of generalized skew-grid dipole array geometry.

x, and thus the only change to the formulation is that $\hat{k}_{ymn}$ is now a function of both m and n, taking the form

$$\hat{k}_{ymn} = \hat{k}_{y0} + \frac{n}{\hat{D}_y} - \frac{m}{\hat{D}_x \tan\xi}. \tag{9}$$

where ξ is the skew angle (see for example [1]). Given the assumptions outlined in the second paragraph of Sec. II-A, a Floquet expansion of the current density associated with a current sheet composed of the dipoles yields

$$K_x(x,y) = \sum_{m=-\infty}^{\infty}\sum_{n=-\infty}^{\infty} K_{mn}\exp\left(-jk\hat{k}_{xm}x\right) \times \exp\left(-jk\hat{k}_{ymn}y\right) \tag{10}$$

where K_{mn} are the expansion coefficients. It is understood that the summation for both m and n is from minus to plus infinity for all cases in this derivation, which has been left out from this point on for the sake of brevity and space. Since the currents are in x only, the fields arising from the current sheet are TM with respect to the x-axis. The electric and magnetic fields associated with this current density are thus

$$E_x(x,y,z) = \sum_m\sum_n E_{xmn}\exp\left(-jk\hat{k}_{xm}x\right) \times \exp\left(-jk\hat{k}_{ymn}y\right)\exp\left(-jk\hat{\kappa}_{mn}z\right) \tag{11a}$$

$$H_y(x,y,z) = \frac{1}{\eta}\sum_m\sum_n \frac{\hat{\kappa}_{mn}}{\hat{k}_{xm}^2-1}E_{xmn}\exp\left(-jk\hat{k}_{xm}x\right) \times \exp\left(-jk\hat{k}_{ymn}y\right)\exp\left(-jk\hat{\kappa}_{mn}z\right) \tag{11b}$$

where H_y is obtained from E_x using a construction of solutions based on TM$_x$ Hertzian potentials (see for example [25]). Enforcing boundary conditions on the plane containing the dipoles yields

$$H_y\big|_{z=0^+} = \frac{1}{2}K_x \tag{12}$$

which can then be combined with (10) and (11), resulting in

$$E_x(x,y,z) = \frac{\eta}{2}\sum_m\sum_n \frac{\hat{k}_{xm}^2-1}{\hat{\kappa}_{mn}}K_{mn}\exp\left(-jk\hat{k}_{xm}x\right) \times \exp\left(-jk\hat{k}_{ymn}y\right)\exp\left(-jk\hat{\kappa}_{mn}z\right) \tag{13}$$

The complex power P_c can be computed by integrating $-\frac{1}{2}(\mathbf{E}\cdot\mathbf{K}^*)$ over a unit cell, yielding

$$P_c = -\frac{\eta\lambda^2\hat{D}_x\hat{D}_y}{4}\sum_m\sum_n \frac{\hat{k}_{xm}^2-1}{\hat{\kappa}_{mn}}|K_{mn}|^2 \tag{14}$$

To solve for K_{mn}, the current distribution is assumed to be cosinusoidal, of the form

$$K_x(x) = \frac{I_0}{\lambda\hat{b}} \cos\frac{\pi x}{\lambda\hat{a}} \tag{15}$$

on the dipoles and zero elsewhere. Equating (10) and (15) and integrating over a unit cell while exploiting orthogonality results in

$$K_{mn} = \frac{2}{\pi} \frac{I_0\hat{a}}{\lambda\hat{D}_x\hat{D}_y} \frac{\sin\left(\pi\hat{k}_{ymn}\hat{b}\right)}{\pi\hat{k}_{ymn}\hat{b}} \frac{\cos\left(\pi\hat{k}_{xm}\hat{a}\right)}{1-\left(2\hat{k}_{xm}\hat{a}\right)^2} \tag{16}$$

The scan impedance Z_S is obtained from the relation

$$P_c = \frac{1}{2}|I_0|^2 Z_S \tag{17}$$

Finally, combining (14), (16),and (17) yields

$$Z_S = \frac{2\eta}{\pi^2} \frac{\hat{a}^2}{\hat{D}_x\hat{D}_y} \sum_m \sum_n F_{mn}^2\, G_m^2\, H_{mn} \tag{18}$$

where F_{mn}, G_m, and H_{mn} are as shown in (2), with the exception of the dependency of F_{mn} on both m and n that follow from the skew grid form of $\hat{k}_{ymn}$. In the case of a rectangular grid, this is no longer the case and both are a function of n only, hence dropping the m subscript.

REFERENCES

[1] N. Amitay, V. Galindo, and C. P. Wu, *Theory and Analysis of Phased Array Antennas*. Wiley-Interscience, 1972.

[2] H. A. Wheeler, "Simple relations derived fom a phased-array antenna made of an infinite current sheet," *IEEE Transactions on Antennas and Propagation*, vol. 13, pp. 506–514, July 1965.

[3] S. Edelberg and A. A. Oliner, "Mutual coupling effects in large antenna arrays: Part i–slot arrays," *IRE Transactions on Antennas and Propagation*, vol. 8, pp. 286–297, May 1960.

[4] J. Allen, "Gain and impedance variation in scanned dipole arrays," *IRE Transactions on Antennas and Propagation*, vol. 10, pp. 566–572, September 1962.

[5] P. J. Meier and H. A. Wheeler, "Dielectric-lined circular waveguide with increased usable bandwidth," *IEEE Transactions on Microwave Theory and Techniques*, vol. 12, pp. 171–175, March 1964.

[6] P. J. Meier, M. A. Balfour, and H. A. Wheeler, "Circular waveguide loaded with dielectric discs for increased usable bandwidth," in *PT-GMTT*, Long Island, NY, USA, May 1964.

[7] R. J. Mailloux, *Phased Array Antenna Handbook*, 2nd ed. Artech House, 2005.

[8] E. G. Magill and H. A. Wheeler, "Wide-angle impedance matching of a planar array antenna by a dielectric sheet," *IEEE Transactions on Antennas and Propagation*, vol. 14, pp. 49–53, January 1966.

[9] N. Marcuvitz, *Waveguide Handbook*. Peregrinus, 1993.

[10] R. E. Collin, *Foundations for Microwave Engineering*, 2nd ed. McGraw-Hill, 1992.

[11] B. Munk, R. Taylor, T. Durham, W. Croswell, B. Pigon, R. Boozer, S. Brown, M. Jones, J. Pryor, S. Ortiz, J. Rawnick, K. Krebs, M. Vanstrum, G. Gothard, and D. Wiebelt, "A low-profile broadband phased array antenna," in *Proceedings of the 2003 IEEE Antennas and Propagation Society International Symposium (APS 2003)*, vol. 2, Columbus, OH, USA, June 2003, pp. 448–451.

[12] S. Sajuyigbe, M. Ross, P. Geren, S. A. Cummer, M. H. Tanielian, and D. R. Smith, "Wide angle impedance matching metamaterials for waveguide-fed phased-array antennas," *IET Microwaves, Antennas & Propagation*, vol. 4, pp. 1063–1072, August 2010.

[13] E. Martini, G. M. Sardi, P. Rocca, G. Oliveri, S. Macii, and A. Massa, "Optimization of metamaterial waim for planar arrays," in *Radio Science Meeting (Joint with AP-S Symposium), (2013 USNC-URSI)*, Lake Buena Vista, FL, USA, July 2013, p. 86.

[14] L. Manica, M. Carlin, I. Malcic, G. Oliveri, and A. Massa, "Wideband multilayer waim design and optimization," in *Proceeding of the 8th European Conference on Antennas and Propagation (EuCAP 2014)*, The Hague, The Netherlands, April 2014, pp. 2997–3000.

[15] G. V. Eleftheriades and K. G. Balmain, *Negative-Refraction Metamaterials: Fundamental Principles and Applications*. John Wiley & Sons and IEEE Press, 2005.

[16] T. R. Cameron, S. V. Hum, and G. V. Eleftheriades, "A wide-angle impedance matching metasurface," in *Proceedings of the 2014 IEEE International Symposium on Antennas and Propagation (APS 2014)*, Memphis, TN, USA, July 2014.

[17] R. C. Hansen, *Microwave Scanning Antennas Vol. II, Array Theory and Practice*. Academic Press, 1966.

[18] L. Stark, "Radiation impedance of a dipole in an infinite planar phased array," *Radio Science*, vol. 1, p. 361377, March 1966.

[19] D. M. Pozar and D. H. Schaubert, "Analysis of an infinite array of rectangular microstrip patches with idealized probe feeds," *IEEE Transactions on Antennas and Propagation*, vol. 32, pp. 1101–1107, October 1984.

[20] R. F. Harrington, *Time-Harmonic Electromagnetic Fields*. Wiley-Interscience, 2001.

[21] A. K. Iyer and G. V. Eleftheriades, "Volumetric layered transmission line metamaterial exhibiting a negative refractive index," *Journal of the Optical Society of America B*, vol. 23, pp. 553–570, March 2006.

[22] M. Selvanayagam and G. V. Eleftheriades, "Circuit modeling of huygens surfaces," *IEEE Antennas and Wireless Propagation Letters*, vol. 12, pp. 1642–1645, 2013.

[23] S. Monni, G. Gerini, A. Neto, and A. G. Tijhuis, "Multimode equivalent networks for the design and analysis of frequency selective surfaces," *IEEE Transactions on Antennas and Propagation*, vol. 55, p. 28242835, October 2007.

[24] L. Stark, "Radiation impedance of a dipole in an infinite planar phased array," *Radio Science*, vol. 1, pp. 361–377, March 1966.

[25] R. E. Collin, *Field Theory of Guided Waves*. McGraw-Hill, 1960.

Trevor Cameron (SM'09) earned the B.Sc. (with Distinction) and M.Sc. degrees from the University of Calgary, Alberta, Canada, in 2009 and 2012, respectively. He is currently pursuing the Ph.D. degree in electrical engineering with the Eleftheriades Waves group at the University of Toronto, Ontario, Canada.

Over the course of his studies he has worked on a variety of topics, which include microwave tissue spectroscopy as well as microstrip, waveguide, and leaky-wave antennas. His current interests include periodic structures, metamaterials, metasurfaces, antenna design, and electromagnetic theory.

Mr. Cameron was awarded the Canada Graduate Scholarship (CGS-M) by the Canadian Institutes of Health Research (CIHR) of Canada in 2009, the Information and Communications Technology (ICT) Graduate Scholarship by the Alberta Informatics Circle of Research Excellence (iCORE) in 2010, and the Canada Graduate Scholarship (CGS-D) by the National Sciences and Engineering Research Council (NSERC) of Canada in 2012. He received an honorable mention in the Student Paper Competition at the 2015 IEEE AP-S Symposium on Antennas and Propagation. From 2009 to 2011, he acted as the Antennas and Propagation liaison for the Southern Alberta COMMTTAP (Communications, Microwave Theory and Techniques, and Antennas and Propagation Societies) Chapter under the guidance of Dr. Elise Fear. He has served as a reviewer for the IEEE Transactions on Antennas and Propagation since 2011.

George V. Eleftheriades (S'86–M'88–SM'02–F'06) earned the M.S.E.E. and Ph.D. degrees in electrical engineering from the University of Michigan, Ann Arbor, MI, USA, in 1989 and 1993, respectively. From 1994 to 1997, he was with the Swiss Federal Institute of Technology, Lausanne, Switzerland. Currently, he is a Professor in the Department of Electrical and Computer Engineering at the University of Toronto, ON, Canada, where he holds the Canada Research/Velma M. Rogers Graham Chair in Nano- and Micro-Structured Electromagnetic Materials. He is a recognized international authority and pioneer in the area of metamaterials. These are man-made materials which have electromagnetic properties not found in nature. He introduced a method for synthesizing metamaterials using loaded transmission lines. Together with his graduate students, he provided the first experimental evidence of imaging beyond the diffraction limit and pioneered several novel antennas and microwave components using these transmission-line based metamaterials. His research has impacted the field by demonstrating the unique electromagnetic properties of metamaterials; used in lenses, antennas, and other microwave and optical components to drive innovation in fields such as satellite communications, defence, medical imaging, microscopy, automotive radar, and wireless telecommunications. Presently, he is leading a group of 12 graduate students and researchers in the areas of electromagnetic and optical metamaterials, and metasurfaces, antennas and components for broadband wireless communications, novel antenna beam-steering techniques, far-field super-resolution imaging, radars, plasmonic and nanoscale optical components, and fundamental electromagnetic theory.

Prof. Eleftheriades served as an Associate Editor for the IEEE TRANSACTIONS ON ANTENNAS AND PROPAGATION (AP). He also served as a member of the IEEE AP-Society administrative committee (AdCom) from 2007 to 2012 and was an IEEE AP-S Distinguished Lecturer from 2004 to 2009. He served as the General Chair of the 2010 IEEE International Symposium on Antennas and Propagation held in Toronto, ON, Canada. Papers that he co-authored have received numerous awards such as the 2009 Best Paper Award from the IEEE MICROWAVE AND WIRELESS PROPAGATION LETTERS, twice the R. W. P. King Best Paper Award from the IEEE TRANSACTIONS ON ANTENNAS AND PROPAGATION (2008 and 2012), and the 2014 Piergiorgio Uslenghi Best Paper Award from the IEEE ANTENNAS AND WIRELESS PROPAGATION LETTERS. His work has been cited more than 10,000 times. He received the Ontario Premier's Research Excellence Award and the University of Toronto's Gordon Slemon Award, both in 2001. In 2004 he received an E.W.R. Steacie Fellowship from the Natural Sciences and Engineering Research Council of Canada. He is the recipient of the 2008 IEEE Kiyo Tomiyasu Technical Field Award and the 2015 IEEE AP-S John Kraus Antenna Award. In 2009, he was elected a Fellow of the Royal Society of Canada.